Material Scaling for Laboratory Experiments of Zoned Dam Breaching due to Overtopping

Conference Paper

Author(s):
Halso, Matthew Christopher; Evers, Frederic M.; Vetsch, David F.; Boes, Robert

Publication date:
2023-08

Permanent link:
https://doi.org/10.3929/ethz-b-000636229

Originally published in:
https://doi.org/10.3850/978-90-833476-1-5_iahr40wc-p0448-cd

Funding acknowledgement:
192223 - Composite modelling of dam breaching due to overtopping (SNF)

40TH IAHR WORLD CONGRESS VIENNA–AUSTRIA 21–25 AUGUST 2023 FROM MOUNTAINS TO COAST

Proceedings of the 40th IAHR World Congress
21-25 August
2023
Vienna, Austria
DOI number

Material Scaling for Laboratory Experiments of Zoned Dam Breaching due to Overtopping

Matthew C. Halso[(1)], Frederic M. Evers, David F. Vetsch, and Robert M. Boes

Laboratory of Hydraulics, Hydrology and Glaciology (VAW), ETH Zurich, Zurich, Switzerland
[(1)] halso@vaw.baug.ethz.ch

Abstract

The overtopping of an embankment dam or dike can result in formation of a breach, which may result in a catastrophic flood. Experimental research on zoned embankment breaching has been rare, and the morphodynamic processes that lead to failure of each zone remain not well-understood. A challenge for experimental research of zoned embankment breaching is scaling from prototype to model scale. Froude scaling of material from prototype earthen embankments results in model material that may not be morphodynamically similar to that of the prototype. This can affect the rate of material erosion and may cause a model zone to fail due to a different process than the corresponding prototype zone. As a reference for this study, a prototype-scale zoned earthen embankment dam has been designed. The prototype dam contains three zones: shell, filter, and core. After assessing multiple methods for scaling that have been used in previous experimental hydraulics research, a model dam was designed and constructed by scaling each material zone based on the expected failure process of the prototype zone. A laboratory overtopping breach experiment of the model dam was then performed. A unique failure process was observed for each zone, beginning with a breach channel forming through the shell due to progressive surface erosion, and ending with the core breaking due to cantilever rotation. The experiment demonstrated that the applied scaling approaches allowed for successful representation of the expected failure processes during the overtopping failure of a zoned embankment dam.

Keywords: dam breach, zoned dam, embankment dam, material scaling, overtopping

1. INTRODUCTION

Embankment structures are used all over the world as dams and dikes. Their water storage enables hydropower production, water supply, flood risk reduction, and other valuable benefits to society. But these benefits come with a risk: the failure of an embankment can have catastrophic consequences to life, property, and infrastructure. Such disasters have occurred several times in recent decades, with notable examples including the 1982 Tous Dam in Spain, the Elbe River levee system in 2002, and the New Orleans levee system in 2005. These systems all breached due to overtopping of the dam or dike crest, as a result of either spillway failure (Tous Dam), storm surge (New Orleans), or riverine flooding (Elbe River).

Overtopping of an embankment can lead to erosion of the embankment material. With sufficient time and energy, the overtopping flow may erode enough material to induce a self-progressing breach expansion, allowing water to flow uncontrolled through the breach. The manner in which a breach forms affects the outflow hydrograph, and thus affects the downstream consequences. Homogeneous earthen embankments, which contain a single material distribution throughout their entire volume, breach due to progressive erosion. The breach outflow gradually increases as the breach enlarges, until the water level decreases due to either reservoir depletion or storm surge recession, or the breach expansion comes to a halt due to a balance of impacting and resisting forces. The breaching of homogeneous earthen embankments has been the focus of numerous experimental studies, as summarized by ASCE/EWRI (2011), Amaral et al. (2020), and others.

Zoned earthen embankments, which contain multiple material zones including a cohesive core, have been the subject of far less experimental research than homogeneous embankments. Studies of zoned embankments have included experiments on zoned fuse-plug spillways (Pugh, 1985; Fletcher & Gilbert, 1992; Schmocker et al., 2013) and two-layer zoned earthen dams (Bornschein, 2014; Sadeghi et al., 2020). These studies observed similar failure processes leading to the breach: failure began with progressive erosion of the outer, non-cohesive zones on the downstream embankment face, while the cohesive core resisted erosion. Continued erosion of the outer layers left the core unsupported on the downstream side. Water pressure and soil pressure from the upstream side became too large for the core to withstand, and it eventually failed by breaking apart.

We build upon this relatively small amount of experimental research on zoned embankment breaching by performing an overtopping experiment of a three-zoned embankment dam. As a reference, we designed a prototype dam that represents a large zoned earthen dam. We then performed a laboratory experiment that represents the prototype-scale dam. This paper describes the process of scaling the prototype dam down to laboratory scale. A variety of possible scaling techniques are discussed, and the scaling of each material zone is described. The erosion processes experienced by each zone during the experiment are also described.

2. PROTOTYPE AND MODEL ZONED DAMS

A reference prototype-scale dam was designed based on three existing zoned dams in Switzerland: Jonenbach Dam in Affoltern am Albis, Aabachweiher Dam in Horgen, and Hühnermatt Dam in Einsiedeln. The designed prototype dam contains three zones: 1) a central vertical core with 5% clay, 37% silt, 50% sand, and 8% gravel (mean grain size $d_m = 0.11$ mm, geometric standard deviation of grain size distribution $\sigma_g = 16.2$); 2) a filter along the downstream side of the core, containing 15% sand and 85% gravel ($d_m = 5$ mm, $\sigma_g = 2.8$); and 3) a shell made of 59% gravel and 41% coarser material ($d_m = 56$ mm, $\sigma_g = 4.1$). The prototype dam has a height $h = 20$ m, face slopes of 2:1 [H:V], a crest width $L_k = 6$ m, and a base length in streamwise direction $L_D = 86$ m. The central core and filter zones both have height $h_c = h_f = 18$ m. The core width is $L_{c,b} = 20$ m at the base, and $L_{c,k} = 8$ m at its crest. The filter width is $L_{f,b} = 3$ m at the base, and $L_{f,k} = 1.5$ m at its crest.

The model dam (subscript *model*) is a laboratory-scale version of the prototype dam, containing the same three zones as the prototype (subscript *prot*). The model dam height is $h = 0.5$ m. The scale factor λ is thus:

$$\lambda = \frac{h_{prot}}{h_{model}} = \frac{20}{0.5} = 40 \qquad [1]$$

The model dam contains a 5-cm deep and 20-cm wide (top width along crest) triangular pilot channel through the crest of the dam, along the centerline of the flume. A schematic representation of the dam, with dimensions of the prototype and model dams, is shown in Figure 1.

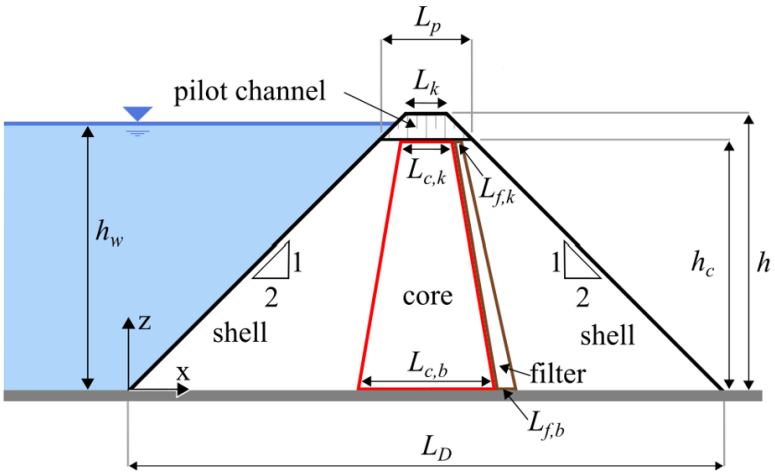

	Prototype [m]	Model [cm]
h	20	50
h_w	19	47.5
h_c	18	45
L_D	86	215
L_k	6	15
L_p	14	35
$L_{c,k}$	8	3.16
$L_{c,b}$	20	7.91
$L_{f,k}$	1.5	3.75
$L_{f,b}$	3	7.5

Figure 1. Schematic of the zoned dam (not to scale) with dimensions of the prototype and model dams.

3. SCALING METHODS

Experimental hydraulic research of free-surface flows typically employs Froude similarity for scaling, meaning that the Froude number – the ratio of inertial and gravitational forces – is the same in model and prototype. Many hydraulic processes are controlled by these forces, and can thus be accurately represented with Froude similarity. Froude similarity scales linear dimensions by the length scale λ; this would include the diameter of embankment material grains d. However, morphodynamic processes, such as sediment transport and material entrainment and deposition, are controlled by drag and turbulence. These forces are related to the Reynolds number – the ratio of inertial and viscous forces – which determines the flow regime. If the Reynolds number in the model gives a different flow regime than that of the prototype, the morphodynamic processes of the model might not be the same as those of the prototype. This can be compensated for by adjusting the model grain size distribution, which requires deviation from scaling d by λ in some cases (Pugh, 1985; Amaral et al., 2020). Several methods for adjustment of model material size have been applied in past experimental hydraulic research, some of which are described in the following sections.

3.1. Critical Shear Velocity

A method for material scaling was developed by Zarn (1992), for use in laboratory experiments investigating a local widening of Switzerland's Emme River. The goal of this method is to scale the critical shear velocity u_c^* [m/s], to ensure that material entrainment is similar in model and prototype. Critical shear velocity for a particle with diameter d [m] and density ρ_s [kg/m^3], in water with density ρ_w [kg/m^3] is defined as:

$$u_c^* = \sqrt{\frac{\theta_c g d(\rho_s - \rho_w)}{\rho_w}} \quad [2]$$

where θ_c [-] is the dimensionless critical shear stress and g [m/s^2] is gravity. According to the Shields Curve (Shields, 1936), θ_c is constant at $\theta_c = 0.047$ for grain Reynolds number $R^* \geq 200$ [-]. For a given shear velocity u^* and fluid kinematic viscosity ν ($\nu_{water} = 10^{-6}$ m^2/s at 20°C), R^* is proportional to d, with:

$$R^* = \frac{u^* d}{\nu} \quad [3]$$

At prototype scale, shear velocity and grain sizes are large enough so that $R^* \gg 200$. But at model scale, R^* may become < 200, and dimensionless critical shear stress will then be $\theta_c \neq 0.047$.

According to Froude similitude, velocities scale with $\sqrt{\lambda}$. It is therefore necessary that:

$$\frac{u_{c,prot}^*}{u_{c,model}^*} = \sqrt{\lambda} \quad [4]$$

Using Eq. [2] for the critical shear velocity of both model and prototype, and cancelling out gravity, water density, and material density (assuming both model and prototype utilize the same material), gives the ratio:

$$\frac{u_{c,prot}^*}{u_{c,model}^*} = \sqrt{\frac{\theta_{c,prot} d_{prot}}{\theta_{c,model} d_{model}}} \quad [5]$$

If model dimensionless critical shear stress $\theta_{c,model} = 0.047$, the θ_c terms can also be cancelled out, and only the grain sizes remain. In this case, with geometric scaling of d, Eq. [5] becomes equal to Eq. [4]. But when $\theta_{c,model} \neq 0.047$, geometric scaling of d does not lead to satisfaction of Eq. [4], and the model grain size d_{model} must be adjusted. Rearranging Eq. [4] shows that it is necessary that:

$$u_{c,model}^* = \frac{u_{c,prot}^*}{\sqrt{\lambda}} \quad [6]$$

To satisfy Eq. [6], a new d_{model} can be selected (and a corresponding $\theta_{c,model}$ given by the Shields Curve) so that $u_{c,model}^*$ (as calculated by Eq. [2]) is equal to the scaled value required by Eq. [6]. This typically increases material size in the finer portion of the model grain size distribution (depending on the hydraulic conditions).

If any portion of the adjusted model grain size distribution remains with $d_{model} < 0.22$ mm, it is removed to reduce cohesive effects in the model. The removed fraction of material is then redistributed to the finer end of the remaining grain size distribution, to retain the same d_m.

3.2. Settling Velocity

A method for scaling of material was presented by Pugh (1985), for use in laboratory experiments of a fuse plug spillway for Oxbow Dam in Idaho, USA (also described in Pugh, 2008). The goal of this method is to accurately scale the material's settling velocity w [cm/s], to ensure that material deposition rates are similar in model and prototype. As stated previously, velocities scale with $\sqrt{\lambda}$. It is therefore necessary that:

$$\frac{w_{prot}}{w_{model}} = \sqrt{\lambda} \quad [7]$$

The settling velocity of earthen material is a function of grain diameter and material density (Dietrich, 1982). For coarser material, settling is controlled by inertial forces and primarily resisted by turbulent drag, resulting in

settling velocity being a function of $\sqrt{d}$. For finer material, settling is controlled by viscous forces and resisted due to laminar drag, resulting in settling velocity being a function of d^2 (Ferguson & Church, 2004). For intermediate material, there is a transition between the two relations. A variety of experimental studies and empirical relations have characterized the transition relationship, as summarized by Dietrich (1982) and Ferguson and Church (2004).

For quartz material (specific weight $\gamma_s = 2.65$), the coarse-grain settling velocity relationship $w = f(\sqrt{d})$ applies for $d > 2$ mm, corresponding to gravel and larger material. The fine-grain relationship $w = f(d^2)$ applies for $d < 0.1$ mm, corresponding to fine sands and smaller material. Medium and coarse sands are in the transition region (Pugh, 1985). Eq. [8] shows the relationship between settling velocity and grain size d [mm] used in the study of Pugh (1985), where both model and prototype material were assumed to be quartz.

for $d > 2.0$ mm:	$w = 11\sqrt{d}$	
for $0.1 \leq d \leq 2.0$ mm:	w determined graphically	[8]
for $d < 0.1$ mm:	$w = 80d^2$	

For geometrically-scaled model material, d scales linearly with λ. Since settling velocity should scale with $\sqrt{\lambda}$, settling velocity is correctly scaled by geometric scaling for model material with $d > 2$ mm.

For model material with $d \leq 2$ mm, w does not scale with $\sqrt{d}$. Therefore, for model material finer than gravel, geometric scaling does not accurately scale the settling velocity. It is necessary to adjust the model grain size d_{model}. Rearranging Eq. [7] shows it is necessary that:

$$w_{model} = \frac{w_{prototype}}{\sqrt{\lambda}} \quad [9]$$

For model material with $d \leq 2$ mm, Eq. [9] can be satisfied through the method of Pugh (1985):

i. For a given d_{prot}, w_{prot} is calculated according to Eq. [8].
ii. w_{prot} is then used to calculate the corresponding w_{model}, from Eq. [9].
iii. d_{model} is selected that corresponds to w_{model}, based on Eq. [8].
iv. Steps (i) to (iii) are repeated for all values of d_{prot} that had been initially geometrically scaled to $d_{model} \leq 2$ mm.

If part of the model grain size distribution remains with $d_{model} < 0.22$ mm after the adjustment of Pugh (1985), it is removed to reduce cohesive effects in the model. The removed fraction of material is then redistributed to the finer end of the remaining grain size distribution, to retain the same d_m.

3.3. Settling Velocity with Substitute Material

Another option for material scaling is similar to the settling velocity method described in Section 3.2, but with a different material used in the model. By using a material with a lower density than quartz ($\gamma_s = 2.65$), the same w_{model} can be achieved at larger grain sizes. This can be especially helpful if scaling with quartz leads to a large portion of the model grain size distribution having $d_{model} < 0.22$ mm, thus needing to be removed and redistributed. Laboratory experiments in which a substitute model material was used have been performed by Roth et al. (2001), Hager and Unger (2010), Beck et al. (2016), and Schäfer et al. (2021).

An equation for settling velocity as a function of material density and shape is given by Hall (2012):

$$w = \left(A + \frac{B}{S_*}\right)^{-1} \sqrt{\left(\frac{\rho_s}{\rho_w} - 1\right) g d} \quad [10]$$

where A and B are coefficients based on the shape and roundness of the material, and S_* is:

$$S_* = \frac{d}{4\nu} \sqrt{\left(\frac{\rho_s}{\rho_w} - 1\right) g d} \quad [11]$$

This method is applied similarly to the settling velocity method described in Section 3.2, with adjustments to steps (iii) and (iv):

i. For a given d_{prot}, w_{prot} is calculated according to Eq. [8].
ii. w_{prot} is then used to calculate the corresponding w_{model}, from Eq. [9].
iii. d_{model} is selected that corresponds to w_{model}, for the substitute material, using Eqs. [10] and [11].
iv. Steps (i) to (iii) are repeated for all values of d_{prot}.

3.4. Layer Thickness

The core of a zoned embankment typically contains cohesive mineral material. The previous studies of zoned embankment overtopping showed that the failure process of a cohesive core zone is different than that of a non-cohesive zone. The core acts as a single cohesive body, rather than as individual grains that experience entrainment and deposition. Failure of the core zone is expected when the momentum load due to water and soil pressures becomes greater than the momentum resistance of the cohesive material. This leads to a cantilever rotational failure, in which large chunks of cohesive material break away from the core (Pugh, 1985; Fletcher & Gilbert, 1992; Schmocker et al., 2013; Sadeghi et al., 2020).

Since failure of a cohesive zone is not due to erosion of individual grains, it is not relevant to scale the grain size. Instead, failure is due to the breaking off of large chunks of cohesive material. These chunks are as thick as the cohesive zone. Therefore, scaling must be based on the thickness of the cohesive zone, while the material size is kept the same between prototype and model (Pugh, 1985).

A method for scaling zones of cohesive material based on layer thickness was presented by Schmocker et al. (2013). The goal of the method is for the model cohesive zone to fail under similar load conditions as the prototype zone. Schmocker et al. (2013) applied the method for laboratory experiments of a fuse plug spillway on Switzerland's Hagneck Canal, which included a clay-containing inclined mineral core. The method was also applied by Sadeghi et al. (2020) for small-scale laboratory experiments representing self-designed prototype zoned dams. A similar method was also described by Pugh (1985). The method of Schmocker et al. (2013) begins with consideration of the momentum load M_L and momentum resistance M_R for a cantilever:

$$M_L = \frac{PL^2}{2} \quad [12]$$

$$M_R = \frac{d_c t^2}{6} f_y \quad [13]$$

where P is a uniform distributed load, L is the length of the cantilever, d_c is the depth of the cantilever along the rotating axis, t is the thickness of the cantilever in the direction of rotation, and f_y is the material ultimate strength. Failure of the core should occur when the momentum load is equal to the momentum resistance. Setting $M_{L,prot} = M_{R,prot}$ and $M_{L,model} = M_{R,model}$ gives:

$$3P_{prot}L_{prot}^2 = d_{c,prot}t_{prot}^2 f_{y,prot} \quad [14]$$

$$3P_{model}L_{model}^2 = d_{c,model}t_{model}^2 f_{y,model} \quad [15]$$

The material type is the same in prototype and model scales. Therefore, f_y is equal in prototype and model. Setting $f_{y,prot} = f_{y,model}$, substituting model parameters for prototype parameters (geometric properties scale with λ, distributed load scales with λ^2), and solving for t_{model} in terms of t_{prot} gives:

$$\frac{3P_{prot}L_{prot}^2}{d_{c,prot}t_{prot}^2} = \frac{3P_{model}L_{model}^2}{d_{c,model}t_{model}^2} \quad [16]$$

$$\frac{3(P_{model}\lambda^2)(L_{model}\lambda)^2}{(d_{c,model}\lambda)t_{prot}^2} = \frac{3P_{model}L_{model}^2}{d_{c,model}t_{model}^2} \quad [17]$$

$$t_{model} = \frac{t_{prot}}{\lambda^{3/2}} \quad [18]$$

As a result of this method, the thickness of a cohesive zone is scaled by $\lambda^{3/2}$, rather than λ. This means the model cohesive zone will be thinner than if it were scaled geometrically. This changes the cross section of the model dam, with the cohesive zone appearing smaller than the other zones relative to prototype scale.

4. APPLICATION OF SCALING METHODS

4.1. Core Zone

The core zone is made of cohesive material (d_m = 0.11 mm, σ_g = 16.2). The method of Schmocker et al. (2013) is the only scaling method considered that is appropriate for cohesive zones. This method was thus applied to the core zone. According to this method, the thickness of the model core should scale according to:

$$t_{model} = \frac{t_{prot}}{\lambda^{3/2}} = \frac{t_{prot}}{40^{3/2}} = \frac{t_{prot}}{253} \quad [19]$$

The core zone is expected to break by rotating in the streamwise direction. Therefore, the thickness t of this scaling method applies to the core streamwise width L_c. The prototype core has a base width $L_{c,b,prot}$ = 20 m and a crest width $L_{c,k,prot}$ = 8 m. At model scale, this scaling method gives a core base width of $L_{c,b,model}$ = 7.91 cm and a crest width $L_{c,k,model}$ = 3.16 cm, instead of a core base width of 50 cm and a core crest width of 20 cm if geometric scaling were used. The scaling method of Schmocker et al. (2013) produces a model core that is over 6 times thinner than it would be with geometric scaling.

4.2. Filter Zone

The prototype filter zone is made of non-cohesive earthen material. The material consists of 15% sand and 85% gravel, with d_m = 5 mm and σ_g = 2.8. With geometric scaling (λ = 40), model material would have d_m = 0.13 mm and σ_g = 2.8, with 73% of the model material finer than 0.22 mm and therefore needing to be removed. The three methods appropriate for non-cohesive material were all considered for this zone.

The substitute material method was considered with plastic grains as the substitute material, as was used by Roth et al. (2001). The plastic has a density of approximately 1030 kg/m^3, which is considerably less than quartz (2650 kg/m^3). The plastic grains in the model filter zone would have a grain size distribution similar to that of the prototype quartz material, with d_m = 5.5 mm, σ_g = 2.3. The largest plastic grains would have $d >$ 20 mm, which is over half the thickness of the filter zone at its crest ($L_{f,k,model}$ = 37.5 mm). This could make construction of the filter zone with the plastic grains quite difficult, and could lead to poor filtration by the filter zone. Therefore, the substitute material method was not selected for the filter zone.

The critical shear velocity scaling method (Zarn, 1992) produced a model filter with d_m = 0.16 mm and σ_g = 2.5. 94% of the model shell material was increased as compared to geometric scaling. Only the coarsest 4% of the material has $R^* > 200$, and thus did not need to be adjusted. The finest 2% of the material actually decreased in size relative to geometric scaling, because for small values of R^*, θ_c is larger than the constant value for $R^* > 200$. Despite the increase in size of most of the material, 70% of the adjusted material size remained with $d <$ 0.22 mm and would need to be removed and redistributed to avoid cohesive effects.

The settling velocity scaling method (Pugh, 1985) produced a model filter with d_m = 0.36 mm and σ_g = 1.7. The entire grain size distribution was increased relative to geometric scaling, because the coarsest material in the geometrically-scaled filter would have $d <$ 2 mm, which is the smallest diameter at which settling velocity scales with $\sqrt{d}$. With all of the model material increased in size, only 15% of the adjusted material would still need to be removed and redistributed to avoid cohesive effects.

The critical shear velocity method and the settling velocity method have both been applied successfully to experiments of embankment breaching due to overtopping, by Schmocker et al. (2013) and Sadeghi et al. (2020), respectively. Both methods are related to important morphodynamic processes – material entrainment for the shear velocity method, material deposition for the settling velocity method – and are thus both relevant for modeling erosion by an overtopping flow. In the study of Schmocker et al. (2013), a 1.2-m tall prototype-scale fuse plug spillway was modeled, with a maximum scale factor of just λ = 5. In the study of Sadeghi et al. (2020), a 10-m high prototype-scale zoned dam was modeled, with λ = 33.33. In that study, the settling velocity method was selected because it produced an adjusted model material that could be mostly retained, without unwanted cohesive effects. In this study, the settling velocity method also produced an adjusted model filter material that could be more retained than the shear velocity method (85% of model material versus 30% does not need to be coarsened). For this reason, the settling velocity method was selected for the filter zone. The filter grain size distributions produced by each scaling method are shown in Figure 2 (prior to the final step of coarsening material with $d <$ 0.22 mm for the critical shear velocity and settling velocity methods).

4.3. Shell Zone

The prototype shell zone is also made of non-cohesive earthen material. The material consists of 59% gravel and 41% cobbles and boulders, with d_m = 56 mm and σ_g = 4.1. With geometric scaling (λ = 40), model

material would have d_m = 1.4 mm and σ_g = 4.1, with 7% of the model material finer than 0.22 mm and therefore needing to be removed and redistributed to avoid cohesive effects. The three methods appropriate for non-cohesive material were considered for the shell zone.

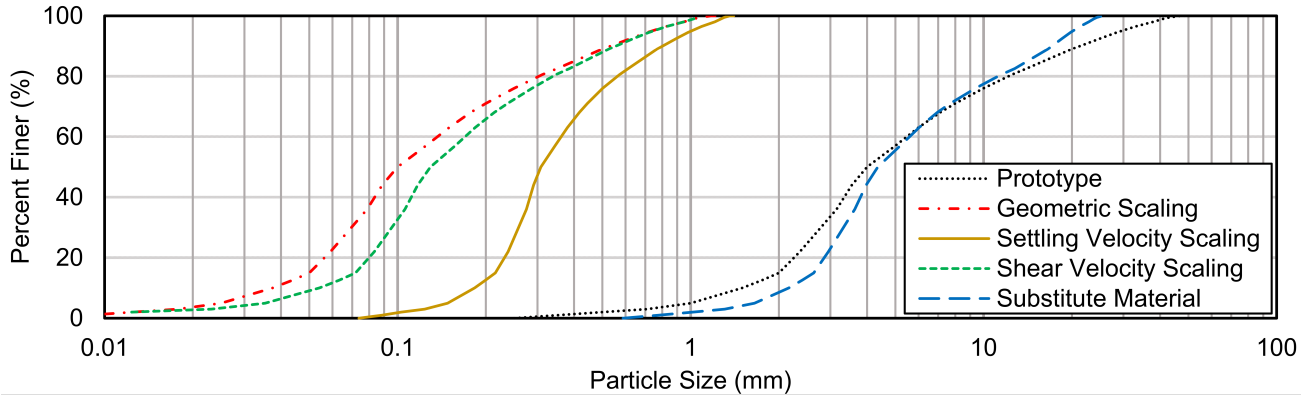

Figure 2. Grain size distributions for the filter zone, including prototype and scaling options.

The substitute material method was again considered with plastic grains for the shell zone. The substitute material for the model shell zone would have a d_m = 30 mm and σ_g = 2.0. But discussions with geotechnical engineers raised questions about the feasibility of building a dam out of such light material. The dam may be too light, and the structure could be pushed downstream by the water pressure from a full reservoir. Therefore, the substitute material method was ruled out for the shell zone.

The critical shear velocity method gives a d_m = 1.44 mm and σ_g = 3.9, increasing the size of 39% of the shell grain size distribution compared with geometric scaling. With this increase, still 5% of the material would need to be removed and redistributed to avoid cohesive effects.

The settling velocity method gives a d_m = 1.78 mm and σ_g = 3.1, increasing the size of 69% of the shell grain size distribution relative to geometric scaling. All material would have an adjusted diameter $d > 0.22$ mm.

The settling velocity method produced an adjusted model shell material that could be more retained than the shear velocity method (5% versus 0% does not need to be coarsened). For this reason, and for consistency with the scaling method applied for the filter zone, the settling velocity method was applied for scaling of the shell zone. The grain size distributions produced by each scaling method (prior to the final step of removing and redistributing material with $d < 0.22$ mm), are shown in Figure 3.

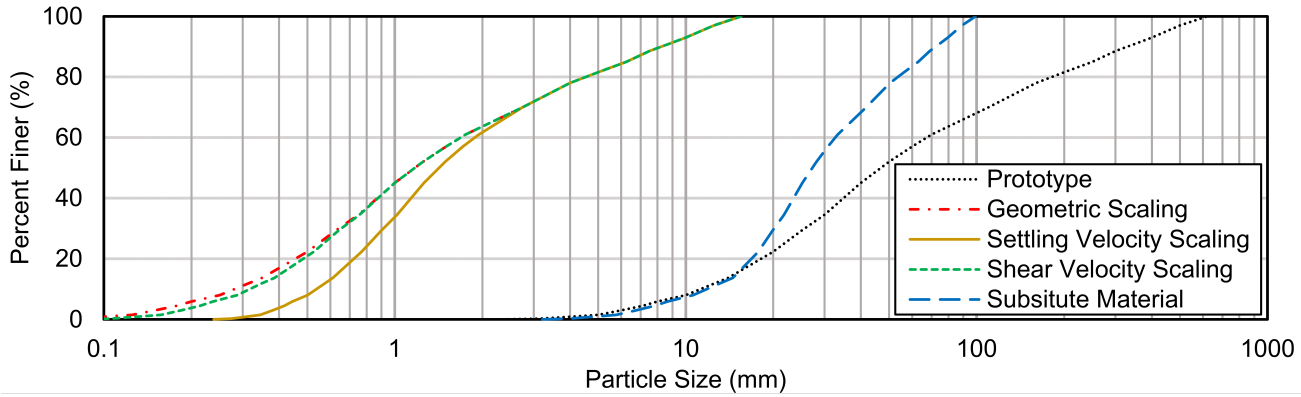

Figure 3. Grain size distributions for the shell zone, including prototype and scaling options.

5. OVERTOPPING DAM BREACH EXPERIMENT

The dam breach experiment was conducted in a 1-m wide, 1-m deep, and 11.9-m long recirculating hydraulic flume. The model dam was constructed on a 0.53-m deep elevated test platform, in the upstream section of the flume. The flume is equipped with systems for measuring reservoir water level, reservoir inflow, seepage flow rate, and weight of eroded material. From these measurements, the breach discharge and erosion rate are calculated. A photogrammetric measurement system was used to track development of the breach. These systems are described by Frank and Hager (2015), Frank (2016), and Halso et al. (2022).

The experiment was initiated by filling the reservoir at approximately 1 mm/s. Once the water level reached h_w = 47.5 cm (2.5 cm above the pilot channel invert, and 2.5 cm below the dam crest), the water level was kept constant. Overtopping of the dam began with flow through the pilot channel. Once the overtopping flow reached

the end of the pilot channel, it began to erode shell material from the downstream face, beginning at the upper end. This erosion led to formation of a breach channel (Figure 4a).

After the front of the breach channel reached the downstream toe (t = 0 s), incision of the breach channel began. Incision began at the upper end of the channel, exposing the crest and part of the downstream face of the core (Figure 4b). Further channel incision led to steep channel side slopes (Figure 4c), which the shell material could not support. The banks collapsed in a series of slope failures (Figure 5), causing shell material to fall into the breach channel, where it was carried away by the overtopping flow. The cycle of incision, mass slope failures, and erosion of slope-failed material drove a progressive lateral expansion of the breach channel.

Figure 4. Progressive surface erosion of shell material leading to (a) initial breach channel, (b) incision of breach channel and core exposure, and (c) further incision of breach channel with unstable side slopes.

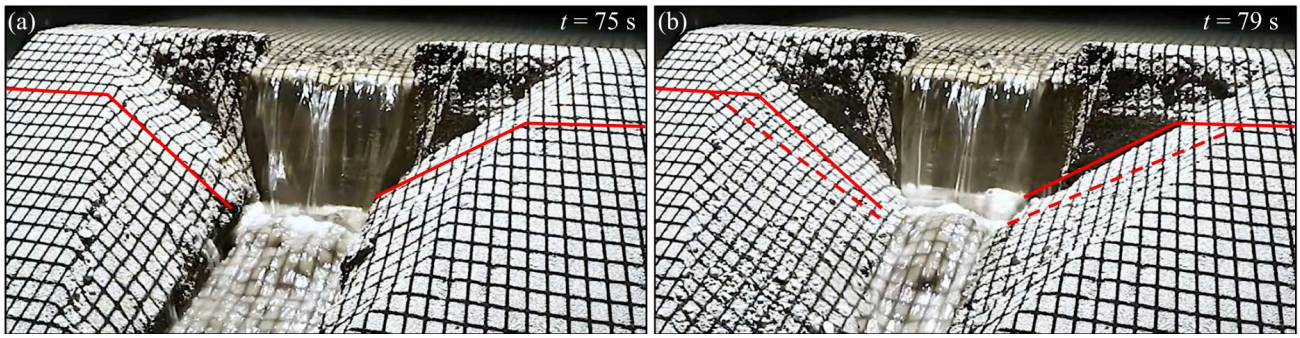

Figure 5. Before (a) and after (b) mass slope failures of shell material on each side of breach channel.

Incision of the breach channel occurred due to surface erosion of the shell material, which is controlled by the sedimentation processes of material entrainment and deposition. The scaling method was based on settling velocity, which is directly related to material deposition. For breach incision, the scaling method appears appropriate. Lateral expansion of the breach channel occurred due to mass slope failures of the shell material, which is controlled by the material angle of repose. The failure angle of dry sand and gravel tends to be in the range of 30-35 degrees, and in homogeneous embankment overtopping experiments with similar setups, has been shown to be fairly independent of material size (Frank & Hager, 2015; Frank, 2016). Therefore, the choice of scaling method likely did not affect the lateral expansion of the breach channel.

Lateral expansion of the breach channel led to exposure of the filter zone. Exposed filter material remained temporarily stable, despite being at a steep angle, likely due to apparent cohesion (Figure 6a). The filter material gradually failed by detachments of apparent-cohesive chunks (Figure 6b), which fell into the breach channel, leaving behind more exposed core area (Figure 6c). Erosion of the filter zone had been expected to be based on surface erosion and slope failures, like the shell zone. The material scaling method was intended to avoid cohesive effects. The filter zone erosion appeared to have been partially controlled by apparent cohesion, therefore it is not clear if this scaling method accurately represented the stability of the filter zone. However, the near-vertical walls that the filter material maintained have been seen in countless prototype, field, and laboratory-scale dam breaches with non-cohesive material, as described and summarized by Amaral et al. (2020) and Rifai et al. (2021). Therefore the failure process of the filter zone may have been accurately depicted.

As the breach channel expanded through incision and mass failures, the core became increasingly unsupported on the downstream side. Water continued to flow over its crest, and soil and water pressures continued to push on it from the upstream side. Despite these stresses, the core remained stable and intact. At time t = 87 s, the pressures from upstream began to push the core downstream, and the core started to bulge in the middle. At t = 103 s, a crack appeared on the downstream face of the core, in the center of the bulge (Figure 7a). At t = 105 s, the core broke along the crack (Figure 7b). The core was pushed open due to cantilever rotation, and a large piece of the core detached from either side of the break, near the lateral extents of the breach channel (Figure 7c). A large breach had thus formed in the dam, and water and shell material from

upstream were able to flow uncontrolled through the breach. This was the expected failure process for the core, and the scaling method was designed for this process. Therefore, the scaling method applied for the core zone seems appropriate. The hydrographs of breach discharge Q_b and material erosion V_e are shown in Figure 8.

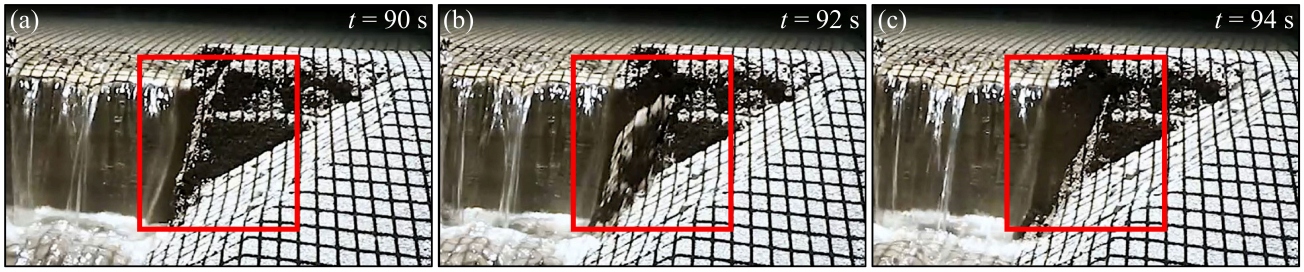

Figure 6. Filter erosion: (a) before, (b) during, and (c) after a mass detachment of apparent-cohesive material.

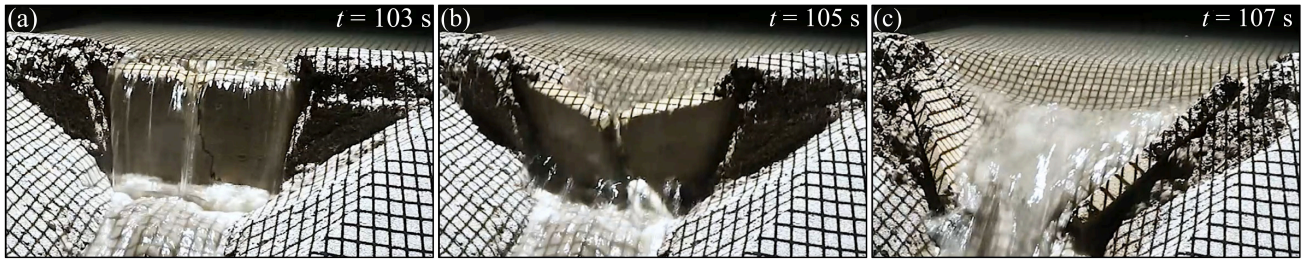

Figure 7. Failure process of core with (a) cracking, (b) breaking along crack, and (c) detachment of large pieces, resulting in a rapid increase in breach outflow.

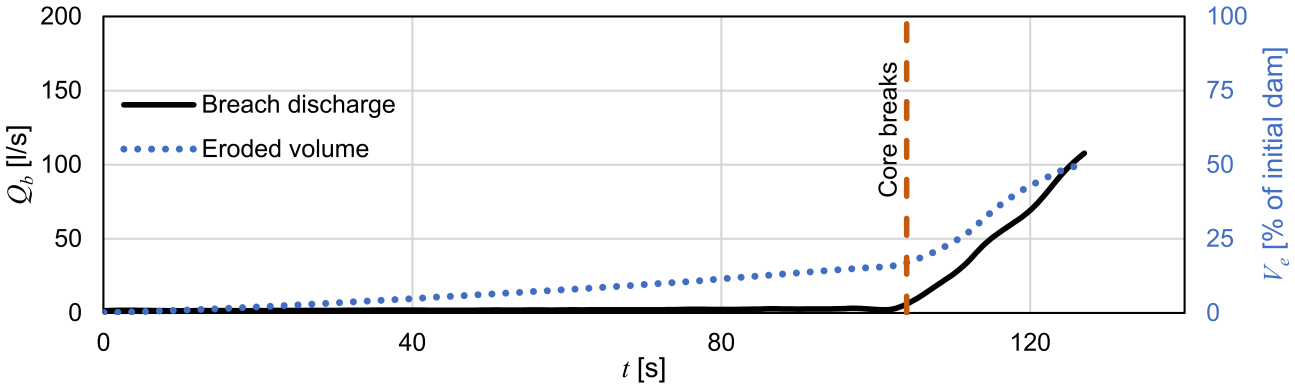

Figure 8. Hydrographs of breach discharge Q_b and eroded material rate V_e during overtopping experiment.

6. CONCLUSIONS

This overtopping breach experiment demonstrated the unique failure process of each zone of a zoned earthen embankment dam. The shell eroded through a combination of progressive surface erosion, which incised the breach channel, and mass slope failures, which expanded the breach channel laterally. The filter was eroded by the overtopping flow and failed by detachments of large apparent-cohesive chunks, which fell into the breach channel. Expansion of the breach channel and removal of filter material left the core unsupported against the forces of water pressure and soil pressure from upstream. These forces caused the core to bulge downstream, crack in the middle of the bulge, and break along the crack. Large pieces of the core detached, forming a large breach in the core. Water and shell material then flowed uncontrolled through the breach.

Each model material zone was scaled for morphodynamic similarity with its corresponding prototype zone. Multiple scaling methods were considered, each designed to accurately scale a process related to morphodynamics: critical shear velocity (Zarn, 1992), settling velocity (Pugh, 1985), settling velocity using substitute material (Roth et al., 2001), and cantilever rotation (Schmocker et al., 2013). The settling velocity method of Pugh (1985), which was designed for non-cohesive zones of embankment material, was applied to the shell and filter zones. These zones were expected to fail with no effects from apparent cohesion. Erosion of the shell zone took place as expected. However, the filter zone appeared to be temporarily stabilized by apparent cohesion. It is not clear if this affected the stability of the core, and thus the timing or magnitude of breach outflow. The cantilever rotation method (Schmocker et al., 2013), which was designed for cohesive mineral cores, was selected for the core zone. The core failed, as expected, through cantilever rotation.

The results from this laboratory experiment help to better understand the processes leading to failure of zoned embankment dams and dikes. The stability of the core against water and soil pressures from upstream can be used to validate statics calculations of core failure. Statics calculations can be implemented in parametric and numerical models of zoned embankment failure, for use by engineers and practitioners in assessing specific prototype zoned dams and dikes. Realization of this experiment can also help to guide the development of experiments with more complex zoning, or experiments representing specific prototype dams.

7. ACKNOWLEDGEMENTS

This study was made possible thanks to funding from the Swiss National Science Foundation (project #192223). Thank you to KIBAG Baustoffe Zurich, for providing material used to make the mineral core.

8. REFERENCES

Amaral, S., Caldeira, L., Viseu, T., & Ferreira, R.M.L. (2020). Designing Experiments to Study Dam Breach Hydraulic Phenomena. *Journal of Hydraulic Engineering*, *146*(4), 04020014.

ASCE/EWRI. (2011). Earthen Embankment Breaching. *Journal of Hydraulic Engineering*, *137*(12), 1549-1564.

Beck, C., Lutz, N., Lais, A., & Boes, R. (2016). Patrind Hydropower Project, Pakistan - Physical model investigation on the optimization of the sediment management concept. *Proc. Hydro 2016 Conference*, Montreux, Switzerland, October 10-12, 2016.

Bornschein, A. (2014). Breschenentwicklung bei Dämmen mit Dichtungen ['Breach development for dams with seals']. *Wasserbauliche Mitteilungen* 50: 303–312, IWD, TU Dresden, Germany (in German).

Dietrich, W.E. (1982). Settling velocity of natural particles. *Water Resources Research*, *18*(6), 1615-1626.

Ferguson, R.I., & Church, M. (2004). A Simple Universal Equation for Grain Settling Velocity. *Journal of Sedimentary Research*, *74*(6), 933-937.

Fletcher, B.P., & Gilbert, P.A. (1992). Center Hill Fuseplug Spillway, Caney Fork River, Tennessee: Hydraulic Model Investigation. Report 92-15, U.S. Army Engineer Waterways Experiment Station.

Frank, P.-J. (2016). Hydraulics of spatial dike breaches. *Doctoral Thesis and VAW Mitteilung* 236 (R. Boes, ed.), VAW, ETH Zurich, Switzerland.

Frank, P.-J., & Hager, W.H. (2015). Spatial dike breach: Sediment surface topography using photogrammetry. *Proc. 36th IAHR World Congress*, The Hague, The Netherlands, June 28 - July 3, 2015.

Hager, W.H., & Unger, J. (2010). Bridge Pier Scour under Flood Waves. *Journal of Hydraulic Engineering*, *136*(10), 842-847.

Hall, S. (2012). Blending and Agitation. In *Rules of Thumb for Chemical Engineers*. Butterworth-Heinemann.

Halso, M.C., Evers, F.M., Vetsch, D.F., & Boes, R.M. (2022). Composite Modeling of the Effect of Material Composition on Spatial Dam Breaching due to Overtopping. *Proc. 39th IAHR World Congress* (M. Ortega-Sánchez, Ed.), Granada, Spain, June 19-24, 2022.

Pugh, C.A. (1985). Hydraulic model studies of fuse plug embankments. Report REC-ERC-85-7, Bureau of Reclamation, US Department of the Interior, Denver.

Pugh, C.A. (2008). Sediment Transport Scaling for Physical Models. In *Sedimentation Engineering: Processes, Measurements, Modeling, and Practice*. 1057-1065. ASCE.

Rifai, I., El Kadi Abderrezzak, K., Hager, W.H., Erpicum, S., Archambeau, P., Violeau, D., Pirotton, M., & Dewals, B. (2021). Apparent cohesion effects on overtopping-induced fluvial dike breaching. *Journal of Hydraulic Research*, *59*(1), 75-87.

Roth, M., Weber, M., & Bezzola, G.R. (2001). Physical Modelling of Sediment Deposits in a River Delta Case study: The Alpenrhein Delta in Lake Constance. *Proc. 29th IAHR Congress*, Beijing, China, September 16-21, 2001.

Sadeghi, S., Hakimzadeh, H., & Amini, A.B. (2020). Experimental Investigation into Outflow Hydrographs of Nonhomogeneous Earth Dam Breaching due to Overtopping. *Journal of Hydraulic Engineering*, *146*(1), 04019049.

Schäfer, S., Fuchs, Y., & Rutschmann, P. (2021). Ähnlichkeit von Sohlformen bei Sand und Leichtgewichts-granulat ['Similarity of Bed Forms for Sand and Lightweight Granules']. *Wasserbau-Symposium and VAW Mitteilung* 236: 409-418 (R. Boes, ed.), VAW, ETH Zurich, Switzerland (in German).

Schmocker, L., Höck, E., Mayor, P.A., & Weitbrecht, V. (2013). Hydraulic Model Study of the Fuse Plug Spillway at Hagneck Canal, Switzerland. *Journal of Hydraulic Engineering*, *139*(8), 894-904.

Shields, A. (1936). Anwendung der Ähnlichkeitsmechanik und der Turbulenzforschung auf die Geschiebebewegung ['Application of similarity laws and turbulence research on sediment movement']. *Doctoral Thesis*, Technical University Berlin, Germany (in German).

Zarn, B. (1992). Lokale Gerinneaufweitung, eine Massnahme zur Sohlenstabilisierung der Emme bei Utzendorf ['Local river widening for bed stabilisation at River Emme in Utzendorf']. *VAW Mitteilung* 118 (D. Vischer, ed.), VAW, ETH Zurich, Switzerland (in German).